

A Unified Earthquake Catalogue of South Asia covering the period 1900-2014

3.1 Introduction

Records of earthquake occurrences, in the form of a catalogue, constitute an important database for seismotectonic and seismic hazard studies. Since the deployment of World-Wide Standard Seismograph Network (WWSSN) during 1963-64, there has been progressive improvement in earthquake data collection. There has been considerable advancement in the data-processing techniques as well as theoretical understanding of the earthquake phenomenon. However, most of the available global and local databases suffer from magnitude type inhomogeneity (*i.e.* usage of different magnitude types), and spatio-temporal heterogeneity in the data completeness. Tackling these issues comprise major objectives towards compilation of unified and reliable earthquake catalogue.

Earliest works of earthquake cataloguing in South Asia (India and the neighboring countries) include Oldham (1883), Tandon and Srivastava (1974), Chandra (1977), Bapat *et al.* (1983), Rao and Rao (1984), & Srivastava and Ramachandran (1985). Quittmeyer and Jacob (1979) reported earthquakes occurred in Pakistan, Afghanistan, Northwest India, and Southeast Iran. Several workers like Lee *et al.* (1976), Gu (1983) amongst many, have catalogued earthquake occurrences in China. The southwestern territory of China falls within the purview of the study region as bounded by latitudes 2° N - 40° N and longitudes 55° E - 102° E. More recently, there have been several efforts to produce homogenous catalogues: Ambraseys and Bilham (2003b) for Afghanistan, Jaiswal and Sinha (2004) for peninsular India, Thingbaijam *et al.* (2008) and Yadav *et al.* (2009) separately for northeast India, and Thingbaijam *et al.* (2009) for Northwest frontier province. In the present study, we looked into four major aspects in order to achieve a consistent earthquake catalogue, *viz.* (1) existing data sources, (2) errors associated with magnitude types, (3) relationships between different magnitude types and applications thereof to homogenize the magnitude entries, and (4) quality of the compiled catalogue in terms of magnitude errors and data completeness.

3.2 Data Sources

We considered three major data sources, namely International Seismological Centre (ISC, <http://www.isc.ac.uk>, last accessed September, 2014), U.S Geological Survey/National Earthquake Information Center (USGS/NEIC, <http://neic.usgs.gov.us>, last accessed September, 2014), and Global Centroid Moment Tensor (GCMT, <http://www.globalcmt.org>, last accessed September, 2014). The annual reporting, as depicted in Figure 3.1, shows that the catalogue from ISC has higher data volume corroborating the similar observation of Willemann and Storchak (2001). This catalogue is, therefore, employed as primary database. Other data sources include India Meteorological Department (IMD, <http://www.imd.gov.in>, last accessed September, 2014) & Jaiswal and Sinha (2004).

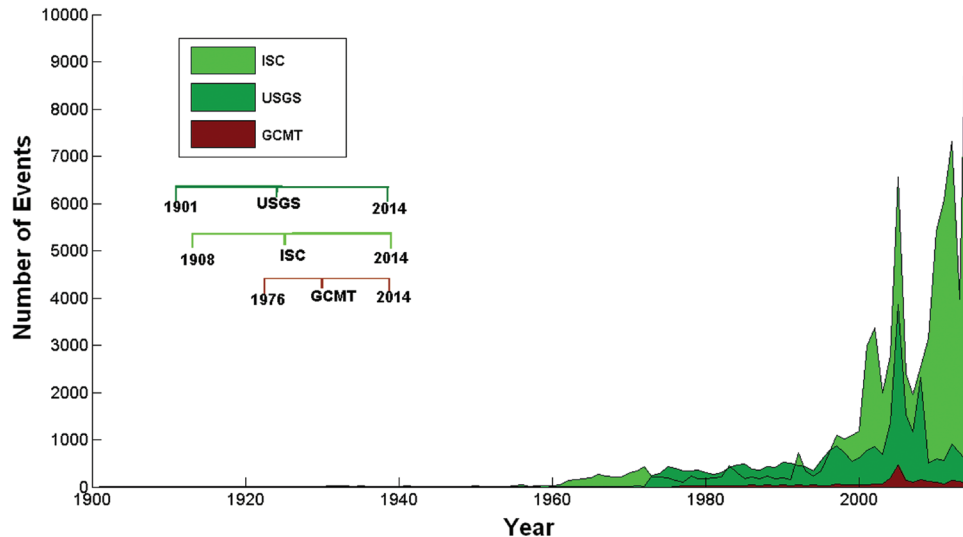


Figure 3.1

Annual reporting of earthquakes with magnitude (all types) ≥ 3.0 in the study region from the three major global agencies: ISC, USGS/NEIC, and GCMT database. The inset depicts the temporal coverage.

Figure 3.2 depicts spatial coverage of the datasets for the different magnitude types. Brief description of the different magnitude types is given in Table 3.1. In the following text, additional subscripts have been used to indicate the data source, *e.g.* $M_{w,JS}$ for the moment magnitude type reported by Jaiswal and Sinha (2004). The dataset for $M_{w,GCMT}$ is derived from the GCMT database, and those for other magnitude types, except $M_{L,IMD}$ and $M_{w,JS}$ are derived from the ISC and USGS catalogues. $M_{w,GCMT}$, $m_{b,ISC}$, $M_{s,ISC}$, M_{ISC} and $M_{L,ISC}$ are widespread although $M_{w,GCMT}$, M_{ISC} and $M_{s,ISC}$ are scanty in the mid-plate regions while $M_{L,ISC}$ is negligible in the Northwest Carlsberg Ridge province. The $m_{pv,ISC}$ specified events are confined to northern parts of the study region in the Hindukush-Pamir province. Events reported in $M_{D,ISC}$ are seen across Northwest and central Himalayas, Andaman-Nicobar and Peninsular India. The $M_{N,ISC}$ specified events are confined in the southwest region. The events from Jaiswal and Sinha (2004) are spatially clustered in south India.

Table 3.1

The different magnitude types used in various earthquake databases (modified after McGuire, 2004)

Magnitude Type	Saturation	Reference
Local/Richter, M_L	~6.8	Richter (1935)
Short period body-wave, m_b	~7.0	Kanamori (1983)
Surface-wave, M_S	~8.0	Gutenberg (1945)
Duration, M_D	N/A [#]	Real and Teng (1973)
Vertical p-wave, m_{pv}	~7.0 [§]	Hori (1969), Bune <i>et al.</i> (1973)
Moment, M_W	None	Hanks and Kanamori (1979)
Lg wave, M_N or M_{bLg}	~7.0 ^ζ	Nuttli (1973)
Vertical surface-wave, M_{Lv}	~8.0 ^ψ	Hori (1969)

[#] Duration magnitudes are used for small earthquakes; [§] based on characteristics of short period P-waves; ^ζ comparable to M_L ; ^ψ vis-à-vis characteristics of surface waves.

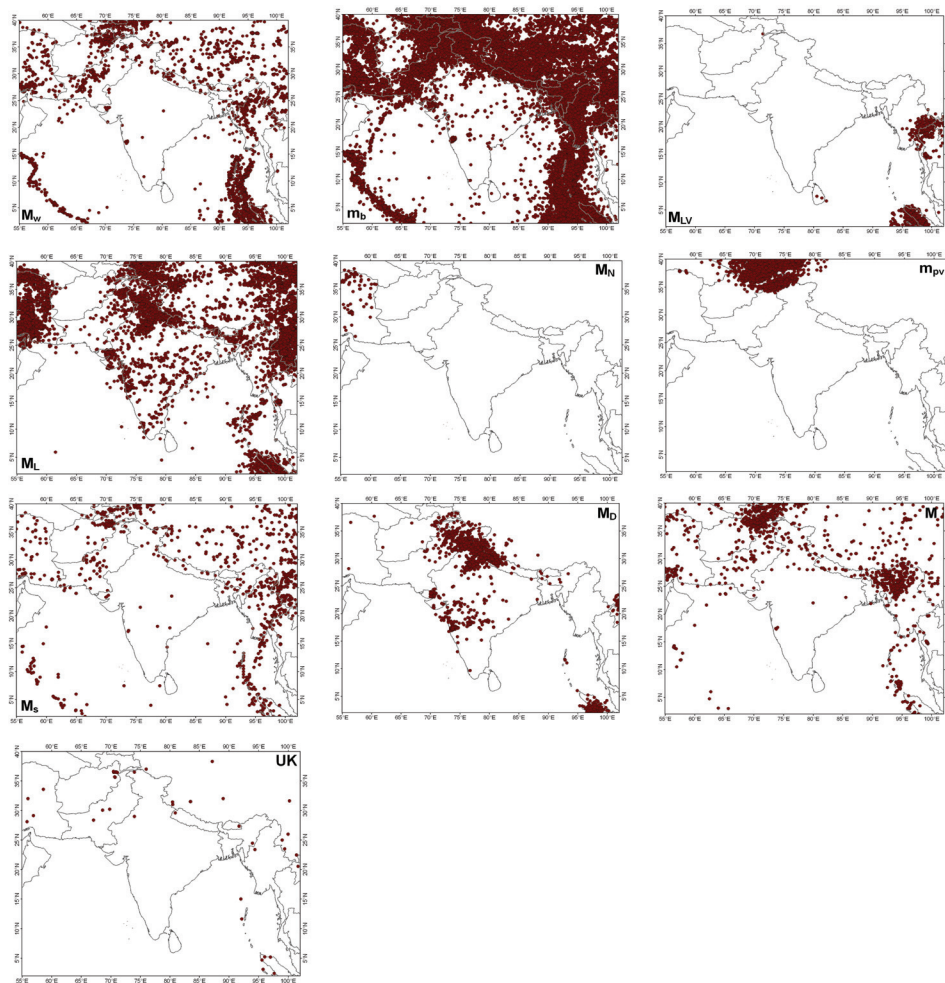


Figure 3.2

Spatial coverage of the derived datasets for the different magnitude types indicated on each map.

3.3 Regression Analyses

The usage of a magnitude type in reporting is decided by several factors such as the recorded data, earthquake source distance from the station deeming to be local, near-field or far-field, *etc.* While moment magnitude (M_w), surface wave magnitude (M_s) and body wave magnitude (m_b) are generally used for teleseismic events, Local magnitude (M_L) and duration magnitude (M_D) are used for local ones. Unification of different magnitude types into a single one is necessary for uniform magnitude scaling. M_w is preferred owing to its applicability for magnitude type which does not suffer from saturation effect unlike other types.

Appropriate relations between different magnitude types through regression analysis are envisaged to develop conversion equations (*e.g.* Castellaro and Bormann, 2007; Bormann *et al.*, 2007; Thingbaijam *et al.*, 2008; 2009; Yadav *et al.*, 2009; Das *et al.*, 2012). Das *et al.* (2012) demonstrated that Orthogonal Standard Regression (OSR) to be more appropriate compared to the standard linear least square technique. In situations necessitating treatment of difference in magnitude errors due to inclusion of non-instrumental data, more complicated approach such as chi-square regression of Stromeyer *et al.* (2004) is warranted. We have employed OSR in the present analysis owing to the use of instrumental dataset and lack of comprehensive error estimation. The detailed derivation of OSR procedure is given in various literatures (*e.g.* Madansky, 1959; Kendall and Stuart, 1979; Fuller, 1987; Carroll and Ruppert, 1996; Castellaro *et al.*, 2006). The OSR method necessitates the understanding of error variance ratio ($\eta = \sigma_y^2 / \sigma_x^2$) which is the ratio of the variables on vertical (dependent) to the horizontal (independent) axes. In the present analysis, we considered the standard deviations of measurement errors as 0.15, 0.20 and 0.25 for $M_{w,GCMT}$, $M_{s,ISC}$ and $m_{b,ISC}$ respectively (Thingbaijam *et al.*, 2008). Due to the non-availability of associated errors for rest of the magnitude scales we considered that the error variance of both the variables are approximately equal leading to a unit error variance

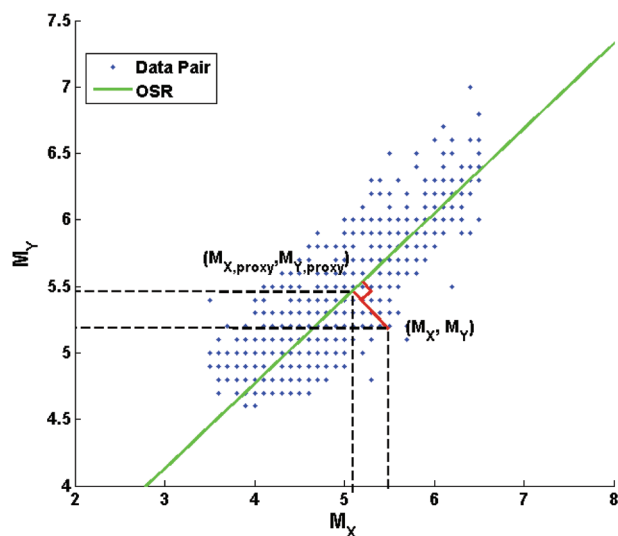


Figure 3.3

Generation of proxy data pairs ($M_{x,proxy}$, $M_{y,proxy}$) by orthogonal projection of (M_x , M_y) on the OSR line.

ratio (e.g. Ambraseys, 1990; Panza *et al.*, 1993; Cavallini and Rebez, 1996; Gutdeutsch *et al.*, 2002; Stromeyer *et al.*, 2004). We have introduced an intermediate step of generating proxy magnitude corresponding to the recorded data to increase the correlation coefficient of the OSR fitting (Das *et al.*, 2012). To estimate proxy data pairs, orthogonal projections have been drawn on the OSR line from the corresponding observed data pairs, as depicted in Figure 3.3. Further these generated proxy data pairs are used to derive OSR relation with the observed data as an intermediate step. The analysis uses linear model of the type: $M_Y = \beta M_X + \alpha$. The fundamental objective is the interchangeability of the variables *i.e.* $M_Y = M_X + \alpha$ and $M_X = M_Y - \alpha$. In case of the expected linear compatibility between the connecting magnitudes, linear fits with slope=1 are also examined (e.g. Braunmiller and Nábelek, 2002).

3.3.1 Relation between $M_{s,ISC}$ and $M_{w,GCMT}$

Surface wave magnitude (M_s) is observed to be consistent for the global catalogues. Frequency plot of 21590 events from ISC catalogue has been constructed for a magnitude range $3.0 \leq M_{s,ISC} \leq 8.7$, for the entire study region during the period 1900-2014 and the plot depicts a bilinear trend as shown in Figure 3.4(a). Thus, the magnitude range has been divided into two subsets, one of which is $3.5 \leq M_{s,ISC} \leq 6.6$, consisting of 2341 events while the other is $6.7 \leq M_{s,ISC} \leq 8.5$ containing 51 events matched respectively with the corresponding $M_{w,GCMT}$ events of GCMT catalogue.

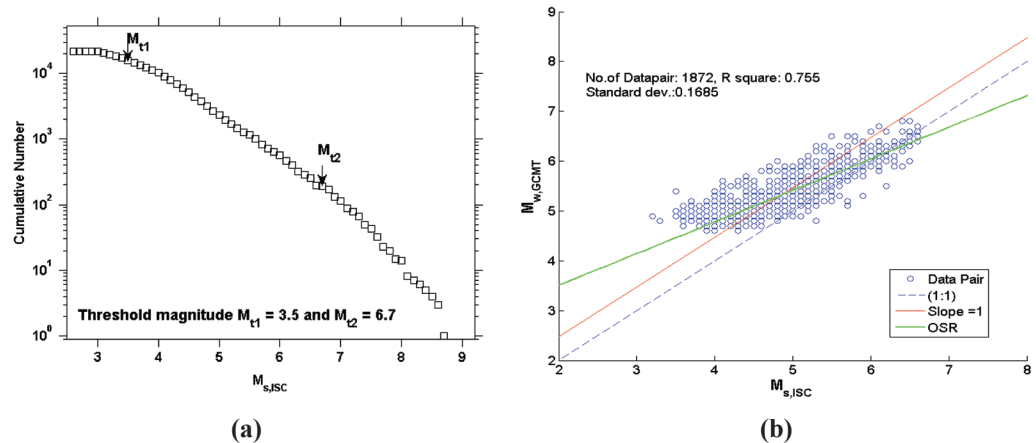


Figure 3.4

(a) Frequency plot of occurrence of $M_{s,ISC}$, and (b) OSR relation between $M_{s,ISC}$ and $M_{w,GCMT}$.

To develop a regression relation between $M_{s,ISC}$ and $M_{w,GCMT}$ for the magnitude range $3.5 \leq M_{s,ISC} \leq 6.6$, we further divided the dataset into two subsets. The first set comprises of 1872 randomly selected events which form about 80% of the total dataset and the second dataset consists of 468 events forming about 20% of the total dataset. The first dataset is used for the development of the OSR relation while the second dataset is used to validate the developed relationship.

The OSR relation, without going through the intermediate step of generating proxy magnitude, between $M_{s,ISC}$ and $M_{w,GCMT}$ as depicted in Figure 3.4(b) is given by

$$M_{w,GCMT} = 0.639 (\pm 0.016) * M_{s,ISC} + 2.211 (\pm 0.0781) \quad (3.1)$$

With $R^2 = 0.755$, $\sigma = 0.1685$ and $\eta = 0.56$.

Where R^2 is the correlation coefficient and σ is the standard deviation.

We then generate the $M_{s,ISC,proxy}$, $M_{w,GCMT,proxy}$ data pair as discussed earlier and worked out the OSR relation between $M_{s,ISC}$ and $M_{s,ISC,proxy}$ as depicted in Figure 3.5(a) given by

$$M_{s,ISC,proxy} = 0.9812 (\pm 0.015) * M_{s,ISC} + 0.0912 (\pm 0.0724) \quad (3.2)$$

with $R^2 = 0.9775$, $\sigma = 0.0192$ and $\eta = 0.56$.

Where $M_{s,ISC,proxy}$ is the abscissa of the point on the OSR line derived from the orthogonal projection of the recorded data point ($M_{s,ISC}$, $M_{w,GCMT}$). Equation (3.2) is the intermediate step followed in deriving the final OSR relation between $M_{s,ISC}$ and $M_{w,GCMT}$. The necessity of using this intermediate step is to improve the correlation coefficient significantly.

The OSR relation between $M_{w,GCMT}$ and the corresponding $M_{s,ISC,proxy}$ as depicted in Figure 3.5(b) is worked out to be

$$M_{w,GCMT} = 0.662 (\pm 0.012) * M_{s,ISC,proxy} + 2.103 (\pm 0.06) \quad (3.3)$$

with $R^2 = 0.8709$, $\sigma = 0.0649$ and $\eta = 0.56$.

From equations (3.2) and (3.3), we finally derived the OSR relationship between $M_{w,GCMT}$ and $M_{s,ISC}$ as given in equation (3.4) below

$$M_{w,GCMT} = 0.6495 * M_{s,ISC} + 2.163 \quad (3.4)$$

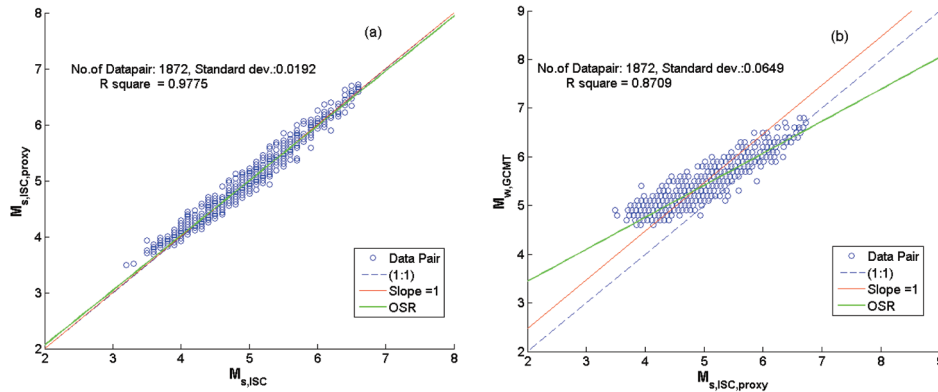


Figure 3.5

(a) OSR relation between $M_{s,ISC}$ and $M_{s,ISC,proxy}$ and (b) OSR relation between $M_{s,ISC,proxy}$ and $M_{w,GCMT}$.

It is evident from equations (3.1), (3.2) and (3.3) that the correlation coefficient has increased significantly by following the intermediate step of generating OSR relation between $M_{w,GCMT}$ and $M_{s,ISC,proxy}$ before achieving the final relation between $M_{w,GCMT}$ and $M_{s,ISC}$.

There are a number of conversion relations already available (e.g. Papazachos *et al.*, 1997; Braunmiller *et al.*, 2005; Scordilis, 2006; Thingbaijam *et al.*, 2008; Yadav *et al.*, 2009; Das *et al.*, 2011) as reported in literatures at regional and global scale. Figure 3.6 depicts the comparison amongst such existing equations as also with the relation derived in the present study. The Log-Likelihood (LLH) methodology worked out the interrelationship among all the conversion relations in terms of rank and weightage as illustrated in the Table 3.2, such that the same can be assigned to each of the equations for the final integration of all the conversion relations in the ultimate conversion of $M_{s,ISC}$ into $M_{w,GCMT}$ within the magnitude range $3.5 \leq M_{s,ISC} \leq 6.6$.

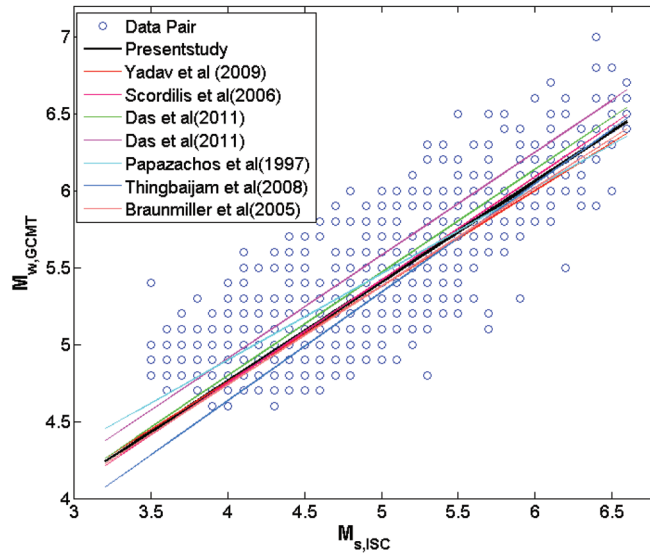


Figure 3.6

Comparison of all the relations between $M_{s,ISC}$ and $M_{w,GCMT}$

Table 3.2

Weightage assigned to different relations according to their fitness to the present dataset

Relations ($M_s - M_w$)	LLH	Weightage	Rank
Present work	1.38372	0.1538	1
Yadav <i>et al.</i> (2009)	1.38749	0.1282	2
Scordilis (2006)	1.39549	0.0897	3
Papazachos <i>et al.</i> (1997)	1.40811	0.0769	4
Das <i>et al.</i> (2011)	1.4135	0.0641	5
Thingbaijam <i>et al.</i> (2008)	1.43016	0.0513	6
Braunmiller <i>et al.</i> (2005)	1.46071	0.0256	7
Das <i>et al.</i> (2011)	1.75066	0.0128	8

The second dataset comprising of 468 events are used to validate the conversion relation derived by considering all the equations with their associated weightage as shown in Table 3.2. The difference between the estimated moment magnitude and the available $M_{w,GCMT}$ is within the limit $-0.4 \leq \Delta M_w \leq 0.4$ as illustrated in Table 3.3.

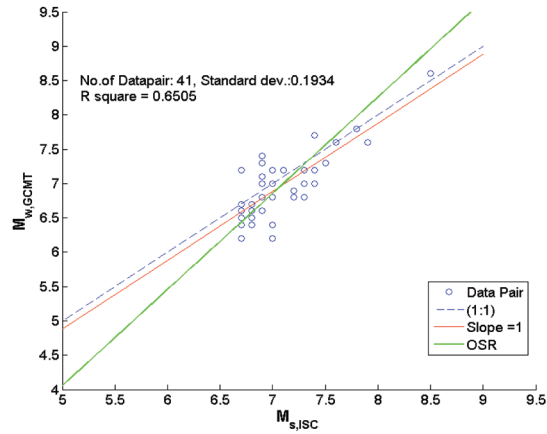


Figure 3.7

OSR relation between $M_{s,ISC}$ and $M_{w,GCMT}$ for magnitude range $6.7 \leq M_{s,ISC} \leq 8.5$.

Similarly, the OSR relation between $M_{s,ISC}$ and $M_{w,GCMT}$ for magnitude range $6.7 \leq M_{s,ISC} \leq 8.5$, without going through the intermediate step is depicted in Figure 3.7 and worked out as

$$M_{w,GCMT} = 1.225 (\pm 0.227) * M_{s,ISC} - 1.642 (\pm 1.562) \quad (3.5)$$

with $R^2 = 0.6505$, $\sigma = 0.1934$ and $\eta = 0.56$.

Table 3.3

Sample presentation of the validation performed for equation (3.4) derived in the present study using 468 events

Event no.	YYYY	MM	DD	hh	mm	sec	Lat (°N)	Long (°E)	Depth (km)	$M_{s,ISC}$	$M_{w,GCMT}$	$M_{w,GCMT}$ derived	Difference (ΔM_w)
1	1976	5	31	5	8	30.5	24.37	98.62	24.5	6.2	6.1	6.2	-0.1
2	1977	1	1	21	39	44	38.19	90.97	42.8	6.2	6	6.2	-0.2
3	1977	4	1	13	36	24.1	27.57	56.30	22.6	6.3	5.9	6.3	-0.4
4	1977	10	13	11	32	9.1	23.47	93.33	60.7	4.9	5.4	5.3	0.1
5	1977	12	19	23	34	33.3	30.93	56.48	26.1	5.7	5.9	5.9	0.0
6	1978	5	24	1	56	10.4	23.83	65.46	29.2	5	5.3	5.4	-0.1
7	1978	8	31	3	26	50.2	27.64	101.15	34.8	5.2	5.3	5.5	-0.2
8	1978	12	18	8	26	20.1	4.20	95.44	70.8	5.2	5.7	5.5	0.2
9	1979	3	10	6	45	8.9	7.53	59.70	10	4.7	5.1	5.2	-0.1
10	1979	9	24	8	46	41.2	36.49	70.16	215.3	4.9	5.2	5.3	-0.1
11	1979	12	2	1	37	10.5	38.50	90.33	23.9	5.4	5.5	5.7	-0.2
12	1980	2	2	12	29	15.3	27.83	101.24	22.3	5.4	5.5	5.7	-0.2
13	1980	4	14	10	17	17.7	36.38	69.58	39.8	5.4	5.5	5.7	-0.2
14	1980	7	12	20	39	34.6	36.88	93.77	20.4	4.9	5.2	5.3	-0.1
15	1980	8	27	4	30	17	15.83	94.67	32	4.9	5.2	5.3	-0.1
16	1980	11	28	21	15	31.2	27.66	56.56	42.8	5.1	5.4	5.5	-0.1
17	1981	4	16	10	27	18.9	27.73	56.37	52.6	4.3	5.1	5.0	0.1
18	1981	6	30	21	55	49.8	22.50	95.19	42.3	4.1	4.9	4.8	0.1
19	1982	1	20	7	9	17.5	7.15	93.88	25.4	6.2	6.1	6.2	-0.1

Event no.	YYYY	MM	DD	hh	mm	sec	Lat (°N)	Long (°E)	Depth (km)	$M_{s,ISC}$	$M_{w,GCMT}$	$M_{w,GCMT}$ derived	Difference (ΔM_w)
20	1982	4	8	2	41	16.9	18.52	86.31	18.2	4.7	5.2	5.2	0.0
21	1982	10	8	13	34	56.9	26.31	100.01	36.1	4.4	5.2	5.0	0.2
22	1983	2	7	15	6	26.6	26.89	57.59	24.5	5.7	5.9	5.9	0.0
23	1983	4	17	23	16	33.8	22.03	94.36	92.6	4.4	5	5.0	0.0
24	1983	8	21	12	6	47.8	3.27	87.50	7.6	4.9	5.4	5.3	0.1
25	1983	10	21	8	44	47.3	22.01	94.38	96.5	4.8	5.2	5.3	-0.1
26	1983	12	8	1	26	22.1	4.33	62.50	10	5.1	5.7	5.5	0.2
27	1984	2	1	14	22	9.2	34.57	70.48	44.5	5.9	6.1	6.0	0.1
28	1984	4	23	21	26	38.9	36.46	70.79	203	5.2	5.5	5.5	0.0
29	1984	7	5	20	48	10.3	11.27	94.76	57.8	4.8	5.2	5.3	-0.1
30	1984	7	10	16	46	49.1	10.93	94.61	19	5.1	5.5	5.5	0.0
31	1984	7	23	2	7	32.6	10.95	94.70	25.3	4.4	5	5.0	0.0

Similarly, the OSR relation between $M_{s,ISC}$ and the corresponding $M_{s,ISC,proxy}$ as depicted in Figure 3.8(a) is given by

$$M_{s,ISC,proxy} = 0.9194 (\pm 0.125) * M_{s,ISC} + 0.555 (\pm 0.8586) \quad (3.6)$$

With $R^2 = 0.8182$, $\sigma = 0.1046$, and $\eta = 0.56$.

The regression relation between $M_{w,GCMT}$ and $M_{s,ISC,proxy}$ as depicted in Figure 3.8(b) is worked out to be

$$M_{w,GCMT} = 1.259 (\pm 0.264) * M_{s,ISC,proxy} - 1.878 (\pm 1.820) \quad (3.7)$$

With $R^2 = 0.9362$ and $\sigma = 0.076$.

From equations (3.6) and (3.7), we finally derived the OSR relationship between $M_{w,GCMT}$ and $M_{s,ISC}$ as given in equation (3.8) below

$$M_{w,GCMT} = 1.157 * M_{s,ISC} - 1.179 \quad (3.8)$$

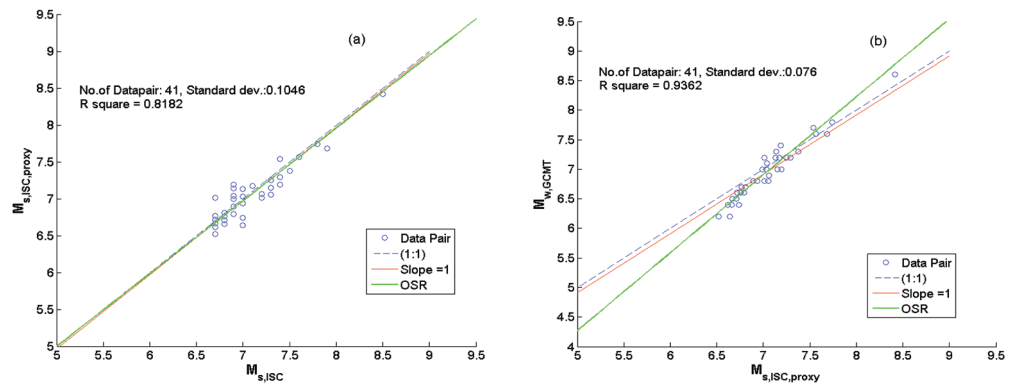


Figure 3.8

(a) OSR relation between $M_{s,ISC}$ and $M_{s,ISC,proxy}$ and (b) OSR relation between $M_{s,ISC,proxy}$ and $M_{w,GCMT}$

It is evident from the equations (3.5), (3.6) and (3.7) that the correlation coefficient has increased significantly by following the intermediate step discussed above.

At the regional as well as global scale, Papazachos *et al.* 1997, Braunmiller *et al.* 2005, Scordilis *et al.* 2006, and Das *et al.* 2011 already reported conversion relations between above concerned magnitude scales for the magnitude range $6.7 \leq M_{s,ISC} \leq 8.5$. Figure 3.9 depicts the comparison amongst such existing equations as also with the relation derived in the present study. Interrelationship among all the conversion relations have been worked out by using LLH methodology in terms of rank and weightage as shown in Table 3.4, such that the same can be assigned to each of the equations for the final integration of all the relations in the ultimate conversion of $M_{s,ISC}$ into $M_{w,GCMT}$ within the magnitude range $6.7 \leq M_{s,ISC} \leq 8.5$.

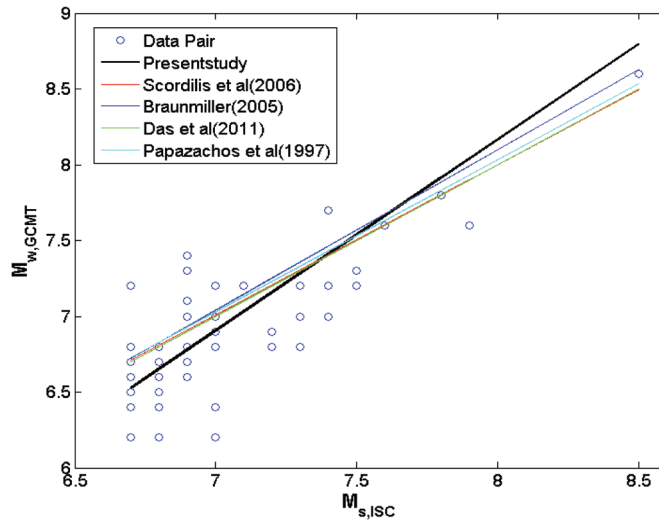


Figure 3.9

Comparison of all the available relations with the present one between $M_{s,ISC}$ and $M_{w,GCMT}$.

Table 3.4

Weightage assigned to different relations according to their fitness to the present dataset

Relations ($M_s - M_w$)	LLH	Weightage	Rank
Present work	1.365885	0.333333	1
Papazachos <i>et al.</i> (1997)	1.367789	0.266667	2
Das <i>et al.</i> (2011)	1.369238	0.2	3
Braunmiller <i>et al.</i> (2005)	1.372186	0.133333	4
Scordilis <i>et al.</i> (2006)	1.374074	0.066667	5

3.3.2 Relation between $M_{s,USGS}$ and $M_{w,GCMCMT}$

Figure 3.10 is a frequency plot of $M_{s,USGS}$ for the magnitude range $4.5 \leq M_{s,USGS} \leq 7.5$ for the entire study region during the period 1900-2014, which depicts a trilinear variation. Thus, the magnitude range has been divided into three segments, first one is of the range $4.5 \leq M_{s,USGS} \leq 5.6$ consisting of 66 events while the second dataset is for the magnitude range $5.7 \leq M_{s,USGS} \leq 7.0$ containing 174 events and the third dataset contains 9 events for the magnitude range $7.1 \leq M_{s,USGS} \leq 7.5$. For the magnitude range $7.1 \leq M_{s,USGS} \leq 7.5$, $M_{s,USGS}$ is equivalent to $M_{w,GCMCMT}$.

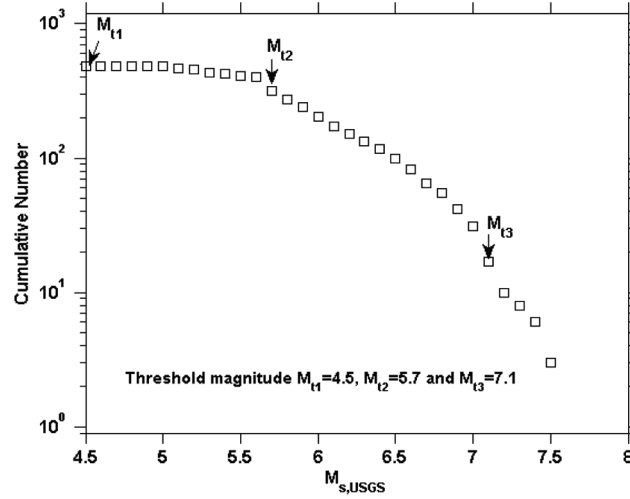


Figure 3.10

Frequency plot of occurrence of $M_{s,USGS}$.

To derive regression relation between $M_{s,USGS}$ and $M_{w,GCMCMT}$ for the magnitude range $4.5 \leq M_{s,USGS} \leq 5.6$, we further divided the dataset into two subsets. The first dataset, comprised of 50 randomly selected events, used for the development of the OSR relation while the second dataset is used to validate the relationship. The OSR relation between $M_{s,USGS}$ and $M_{s,USGS,proxy}$ as depicted in Figure 3.11(a) is worked out as

$$M_{s,USGS,proxy} = 0.9459 (\pm 0.262) * M_{s,USGS} + 0.2958 (\pm 1.434) \quad (3.9)$$

With $R^2 = 0.899$, $\sigma = 0.0095$ and $\eta = 1.0$.

The OSR relation between $M_{w,GCMCMT}$ and corresponding $M_{s,USGS,proxy}$ as depicted in Figure 3.11(b) is worked out to be

$$M_{w,GCMCMT} = 1.216 (\pm 0.332) * M_{s,USGS,proxy} - 0.988 (\pm 1.815) \quad (3.10)$$

With $R^2 = 0.945$ and $\sigma = 0.0091$.

From equations (3.9) and (3.10), we finally derived the OSR relationship between $M_{w,GCMCMT}$ and $M_{s,USGS}$ as given in equation (3.11) below

$$M_{w,GCMCMT} = 1.15 * M_{s,USGS} - 0.6283 \quad (3.11)$$

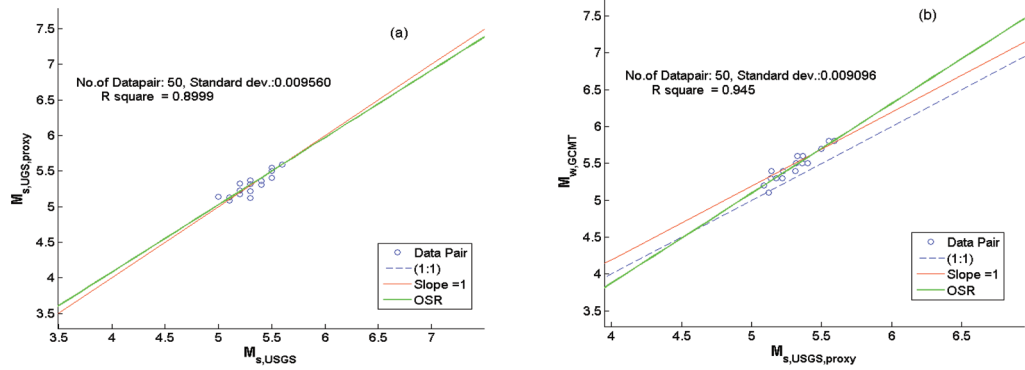


Figure 3.11

(a) OSR relation between $M_{s,USGS}$ and $M_{s,USGS,proxy}$, and (b) OSR relation between $M_{s,USGS,proxy}$ and $M_{w,GCMT}$.

Similarly, the OSR relation between $M_{s,USGS}$ and $M_{s,USGS,proxy}$ for the magnitude range $5.7 \leq M_{s,USGS} \leq 7.0$ as depicted in Figure 3.12(a) is given by

$$M_{s,USGS,proxy} = 0.998 (\pm 0.008) * M_{s,USGS} + 0.011 (\pm 0.052) \quad (3.12)$$

With $R^2 = 0.9964$, $\sigma = 0.0035$ and $\eta = 1.0$.

The OSR relation between $M_{w,GCMT}$ and the corresponding $M_{s,USGS,proxy}$ as depicted in Figure 3.12(b) is worked out to be

$$M_{w,GCMT} = 1.224 (\pm 0.097) M_{s,USGS,proxy} - 1.461 (\pm 0.599) \quad (3.13)$$

With $R^2 = 0.9918$ and $\sigma = 0.0121$.

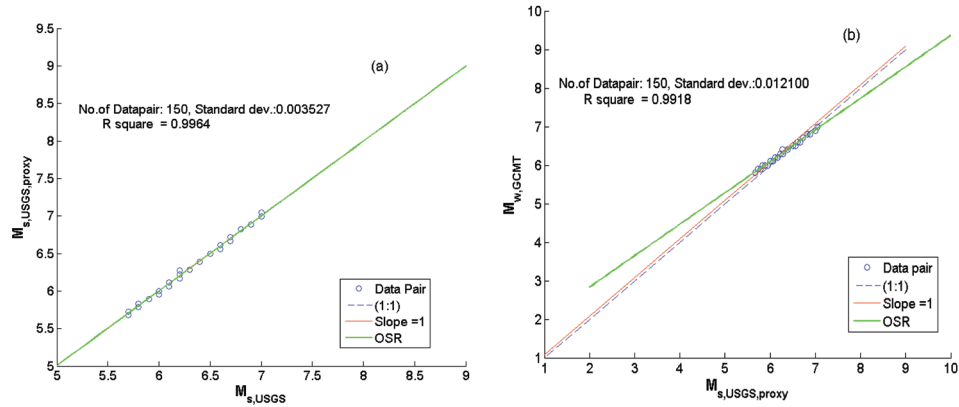


Figure 3.12

(a) OSR relation between $M_{s,USGS}$ and $M_{s,USGS,proxy}$ and (b) OSR relation between $M_{s,USGS,proxy}$ and $M_{w,GCMT}$.

From equations (3.12) and (3.13), we finally derived the OSR relationship between $M_{w,GCMT}$ and $M_{s,USGS}$ as given in equation (3.14) below

$$M_{w,GCMT} = 1.21 * M_{s,USGS} - 1.45 \quad (3.14)$$

3.3.3 Relation between $M_{w,GCMT}$ and Body Wave Magnitude (m_b) of ISC and USGS

To develop OSR relation between $m_{b,ISC}$ and $M_{w,GCMT}$ for the magnitude range $3.8 \leq m_{b,ISC} \leq 7.0$, we separated the dataset into two subsets: first dataset consisting of 1784 randomly selected events for regression and the second dataset containing 467 events are employed to validate the equation derived. Now the OSR relations as depicted in Figure 3.13(a-b) are worked out as

$$m_{b,ISC,proxy} = 0.91 (\pm 0.031) * m_{b,ISC} + 0.463 (\pm 0.158) \quad (3.15)$$

With $R^2 = 0.8744$, $\sigma = 0.0299$ and $\eta = 0.36$.

$$M_{w,GCMT} = 1.277 (\pm 0.055) * m_{b,ISC,proxy} - 1.254 (\pm 0.284) \quad (3.16)$$

With $R^2 = 0.9348$ and $\sigma = 0.0253$.

From equations (3.15) and (3.16) we finally derived the OSR relationship between $m_{b,ISC}$ and $M_{w,GCMT}$ as given in equation (3.17) below.

$$M_{w,GCMT} = 1.16 * m_{b,ISC} - 0.663 \quad (3.17)$$

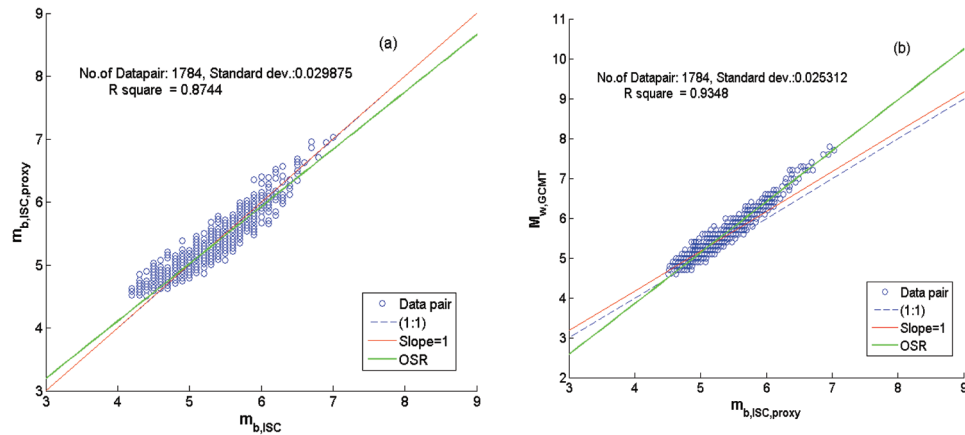


Figure 3.13

(a) OSR relation between $m_{b,ISC}$ and $m_{b,ISC,proxy}$ and (b) OSR relation between $m_{b,ISC,proxy}$ and $M_{w,GCMT}$.

A number of pre-existing conversion relations are reported in different literatures (e.g. Papazachos *et al.*, 1997; Braunmiller *et al.*, 2005; Scordilis, 2006; Thingbaijam *et al.*, 2008; Ristau, 2009; Das *et al.*, 2011; Das *et al.*, 2012) at regional and global scale. Figure 3.14 depicts the comparison between the existing equations and the relation derived in the present study. Thereafter, the Log Likelihood (LLH) method has been used to assign the weightage for the corresponding relations according to their LLH values as illustrated in Table 3.5.

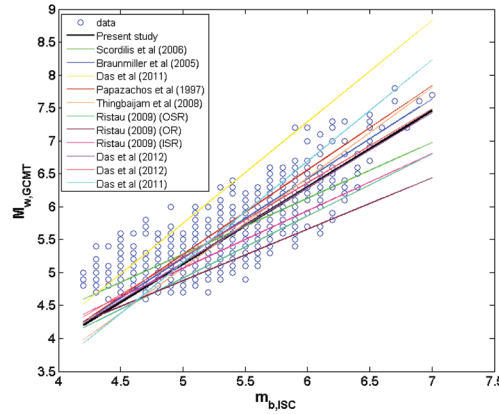


Figure 3.14

Comparison of all the relations between $m_{b,ISC}$ and $M_{w,GCMT}$.

Table 3.5

Weightage assigned to different relations according to their fitness to the present dataset

Relations (m_b - M_w)	LLH	Weightage	Rank
Present work	1.38372	0.1538	1
Das <i>et al.</i> (2012)	1.38612	0.1410	2
Scordilis (2006)	1.38749	0.1282	3
Das <i>et al.</i> (2012)	1.39009	0.1154	4
Ristau (2009) (ISR)	1.39081	0.1026	5
Braunmiller <i>et al.</i> (2005)	1.39549	0.0897	6
Thingbaijam <i>et al.</i> (2008)	1.40811	0.0769	7
Papazachos <i>et al.</i> (1997)	1.4135	0.0641	8
Ristau (2009) (OSR)	1.43016	0.0513	9
Das <i>et al.</i> (2011)	1.43393	0.0385	10
Ristau (2009) (SR)	1.46071	0.0256	11
Das <i>et al.</i> (2011)	1.75066	0.0128	12

Similarly, for the development of OSR relation between $m_{b,USGS}$ and $M_{w,GCMT}$ for the magnitude range $4.6 \leq m_{b,USGS} \leq 6.4$, we have separated out the dataset into two subsets: first dataset consisting of 244 events selected at random are used to generate regression relation and the second dataset containing 50 events are used for the validation of the equation derived. Thus, the OSR relations as depicted in Figure 3.15 are worked out to be

$$m_{b,USGS,proxy} = 0.792 (\pm 0.119) * m_{b,USGS} + 1.061 (\pm 0.6108) \quad (3.18)$$

With $R^2 = 0.7535$, $\sigma = 0.0234$ and $\eta = 1$.

$$M_{w,GCMT} = 1.37 (\pm 0.381) * m_{b,USGS,proxy} - 1.865 (\pm 1.94) \quad (3.19)$$

With $R^2 = 0.8539$ and $\sigma = 0.0185$.

From equation (3.18) and (3.19) we finally derived the relation between $m_{b,USGS}$ and $M_{w,GCMT}$ as given by

$$M_{w,GCMT} = 1.082 * m_{b,USGS} - 0.4128 \quad (3.20)$$

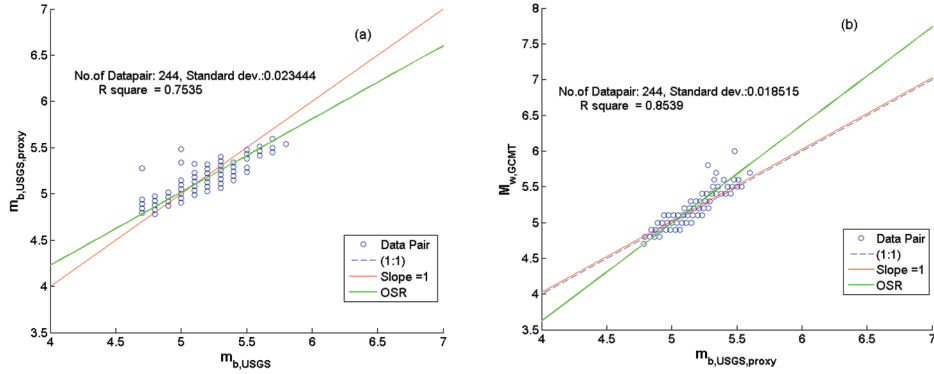


Figure 3.15

(a) OSR relation between $m_{b,USGS}$ and $m_{b,USGS,proxy}$, and (b) OSR relation between $m_{b,USGS,proxy}$ and $M_{w,GCMT}$.

3.3.4 Relation between $M_{L,ISC}$ and $M_{w,GCMT}$

Similarly, a regression relation between $M_{L,ISC}$ and $M_{w,GCMT}$ has been derived for the magnitude range $3.5 \leq M_{L,ISC} \leq 7.3$, for this we have divided the dataset into two subsets. The first dataset comprises of 1114 randomly selected events and the second dataset consists of 282 events. The first dataset is used for the development of the OSR relation while the second dataset is used to validate the relationship.

Now, the OSR relations between $M_{L,ISC}$ and $M_{w,GCMT}$ as depicted in Figure 3.16 are worked out as

$$M_{L,ISC,proxy} = 0.9786 (\pm 0.0078) * M_{L,ISC} + 0.1018 (\pm 0.0377) \quad (3.21)$$

With $R^2 = 0.9753$, $\sigma = 0.02$ and $\eta = 1$.

$$M_{w,GCMT} = 0.5109 (\pm 0.048) * M_{L,ISC,proxy} + 2.83 (\pm 0.232) \quad (3.22)$$

With $R^2 = 0.3286$ and $\sigma = 0.1214$.

Solving equations (3.21) and (3.22) we get the final regression relation as

$$M_{w,GCMT} = 0.499 * M_{L,ISC} + 2.88 \quad (3.23)$$

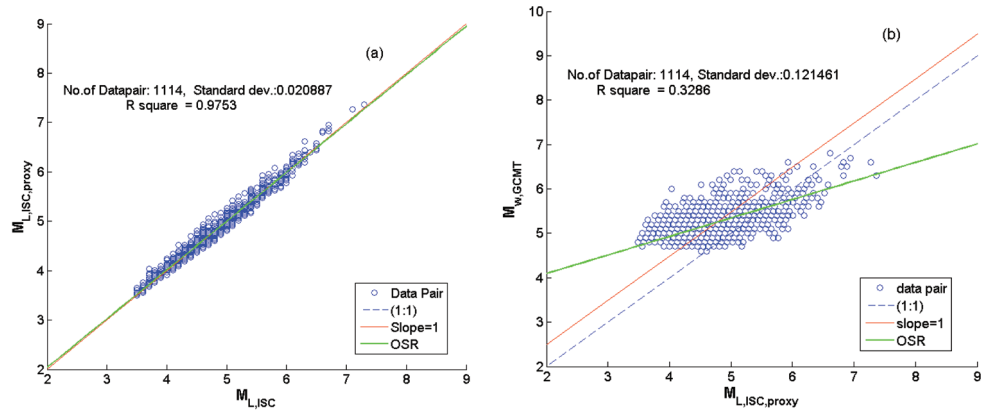


Figure 3.16

(a) OSR relation between $M_{L,ISC}$ and $M_{L,ISC,proxy}$ and (b) OSR relation between $M_{L,ISC,proxy}$ and $M_{w,GCMT}$.

Papazachos *et al.* (1997), Braunmiller *et al.* (2005), Scordilis (2006), Thingbaijam *et al.* (2008), Yadav *et al.* (2009) and Das *et al.* (2011) have already reported conversion relations between $M_{L,ISC}$ and $M_{w,GCMT}$ at both the regional and global scale. A comparison between the relations derived in the present study with the existing equations has been depicted in Figure 3.17. However, the Log Likelihood (LLH) method has been employed to assign the weightage for the corresponding relations according to their LLH values as shown in the Table 3.6.

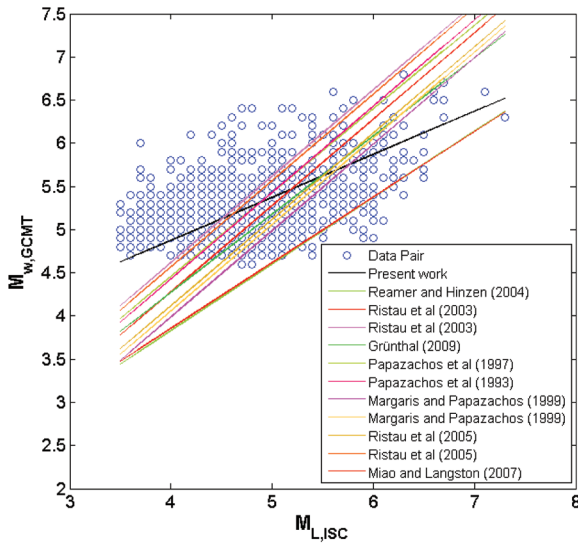


Figure 3.17

Comparison of all the relations between $M_{L,ISC}$ and $M_{w,GCMT}$.

Table 3.6

Weightage assigned to different relations according to their fitness to the present dataset

Relations (M_L-M_w)	LLH	Weightage	Rank
Present work	1.421084	0.1538	1
Papazachos <i>et al.</i> (1997)	1.554382	0.1410	2
Papazachos <i>et al.</i> (1993)	1.567656	0.1282	3
Ristau <i>et al.</i> (2005)	1.570974	0.1154	4
Ristau <i>et al.</i> (2003)	1.579012	0.1026	5
Grünthal (2009)	1.584304	0.0897	6
Ristau <i>et al.</i> (2003)	1.59548	0.0769	7
Ristau <i>et al.</i> (2005)	1.660937	0.0641	8
Margaris and Papazachos (1999)	1.695006	0.0513	9
Margaris and Papazachos (1999)	1.741316	0.0385	10
Miao and Langston (2007)	1.948453	0.0256	11
Reamer and Hinzen (2004)	1.97352	0.0128	12

3.3.5 Magnitude Conversion of $m_{w,USGS}$ to $M_{w,GCMT}$

Frequency plot of $m_{w,USGS}$ has been drawn for a magnitude range $5.1 \leq m_{w,USGS} \leq 7.8$ consisting of 1424 events for the entire study region during the period 1900-2014 and the plot depicts a bilinear trend. Therefore, the magnitude range has been divided into two subsets, one of which is $5.1 \leq m_{w,USGS} \leq 7.0$ consisting of 1412 events while the other is $7.1 \leq m_{w,USGS} \leq 7.8$ containing 12 events.

The OSR relations for the magnitude range $5.1 \leq m_{w,USGS} \leq 7.0$ depicted in Figure 3.18 are worked out to be

$$m_{w,USGS,Proxy} = 0.9957 (\pm 0.0065) * m_{w,USGS} + 0.0228 (\pm 0.0277) \quad (3.24)$$

With $R^2 = 0.9917$, $\sigma = 0.0053$ and $\eta = 1.0$.

$$M_{w,GCMT} = 1.022 (\pm 0.0095) * m_{w,USGS,proxy} - 0.142 (\pm 0.0517) \quad (3.25)$$

With $R^2 = 0.9922$ and $\sigma = 0.0054$.

From equations (3.24) and (3.25), we finally derived the OSR relationship between $M_{w,GCMT}$ and $m_{w,USGS}$ as given in equation (3.26) below

$$M_{w,GCMT} = 1.017 * m_{w,USGS} - 0.118 \quad (3.26)$$

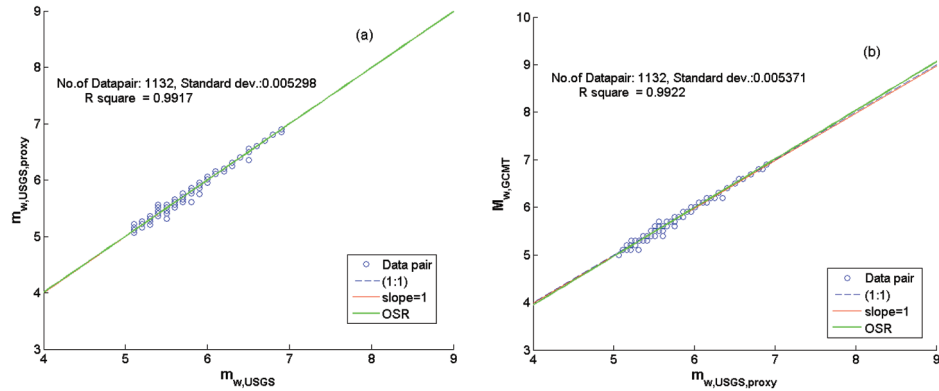


Figure 3.18

(a) OSR relation between $m_{w,USGS}$ and $m_{w,USGS,proxy}$ and (b) OSR relation between $m_{w,USGS,proxy}$ and $M_{w,GCMT}$.

Figure 3.19 depicts the comparison between the existing equation of Scordilis (2006) and the relation derived in the present study. The LLH methodology works out the interrelationship between the conversion relations in terms of rank and weightage as shown in Table 3.7, such that the same can be assigned to both of the equations for the final integration of the relations in the ultimate conversion of $m_{w,USGS}$ into $M_{w,GCMT}$ within the magnitude range $5.1 \leq m_{w,USGS} \leq 7.0$.

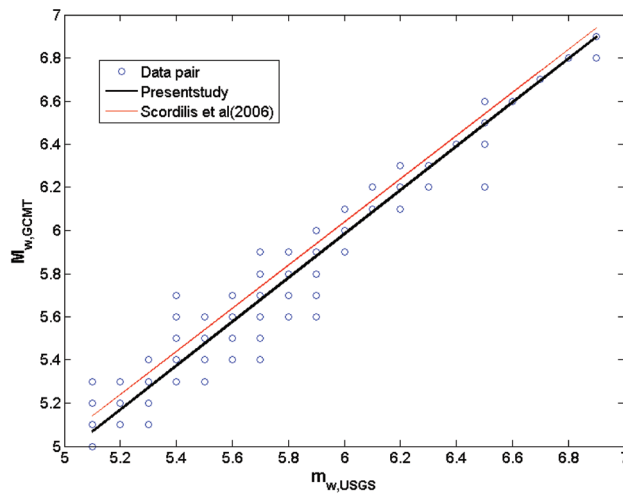


Figure 3.19

Comparison of all the relations between $m_{w,USGS}$ and $M_{w,GCMT}$.

Table 3.7

Weightage assigned to different relations according to their fitness to the present dataset

Relations ($M_s - M_w$)	LLH	Weightage	Rank
Present work	1.3279	0.67	1
Scordilis (2006)	1.3307	0.33	2

For the magnitude range $7.1 \leq m_{w,USGS} \leq 7.8$ consisting of 12 events in the study region, both the $m_{w,USGS}$ and $M_{w,GCMT}$ entries are exactly equivalent.

3.3.6 Relation between $M_{D,ISC}$ and $m_{b,ISC}$

Owing to the insufficiency of events for regression between $M_{D,ISC}$ and $M_{w,GCMT}$ an indirect connectivity through $m_{b,ISC}$ has been made. Thus, the OSR relations between $M_{D,ISC}$ and $m_{b,ISC}$ for the magnitude range $4.0 \leq M_{D,ISC} \leq 6.2$ depicted in Figure 3.20 is worked out as

$$M_{D,ISC,proxy} = 0.6897 (\pm 0.085) * M_{D,ISC} + 1.429 (\pm 0.379) \quad (3.27)$$

With $R^2 = 0.829$ and $\sigma = 0.0382$ and $\eta = 1.0$.

$$m_{b,ISC} = 2.07 (\pm 0.16) * M_{D,ISC,proxy} - 5.14 (\pm 0.722) \quad (3.28)$$

With $R^2 = 0.742$ and $\sigma = 0.0699$.

Solving equations (3.27) and (3.28) we get the final regression relation as

$$m_{b,ISC} = 1.428 * M_{D,ISC} - 2.182 \quad (3.29)$$

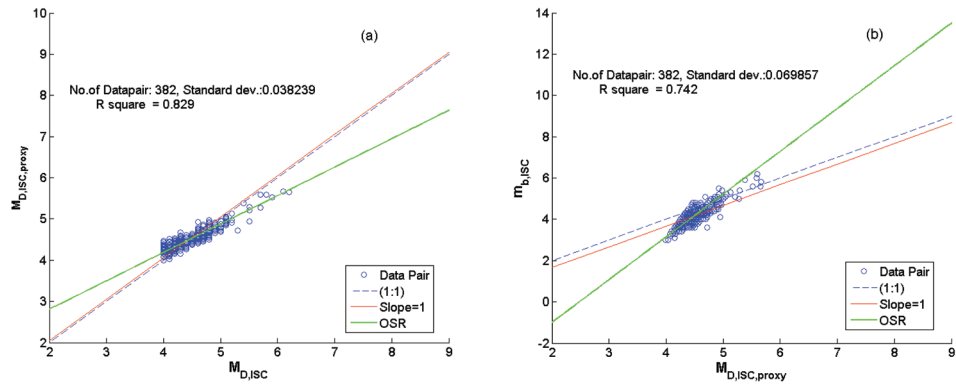


Figure 3.20

(a) OSR relation between $M_{D,ISC}$ and $M_{D,ISC,proxy}$ and (b) OSR relation between $M_{D,ISC,proxy}$ and $m_{b,ISC}$.

3.3.7 Relation of $M_{N,ISC}$ with $M_{L,ISC}$

The OSR relation for conversion of $M_{N,ISC}$ into $M_{L,ISC}$ for magnitude range $3.6 \leq M_{N,ISC} \leq 5.3$ depicted in Figure 3.21 is worked out to be

$$M_{N,ISC,proxy} = 0.9277 (\pm 0.075) * M_{N,ISC} + 0.2953 (\pm 0.297) \quad (3.30)$$

With $R^2 = 0.9358$, $\sigma = 0.0192$ and $\eta = 1.0$.

$$M_{L,ISC} = 1.314 (\pm 0.141) * M_{N,ISC,proxy} - 1.36 (\pm 0.55) \quad (3.31)$$

With $R^2 = 0.9320$ and $\sigma = 0.0321$.

From equations (3.30) and (3.31) we finally derived the OSR relationship between $M_{N,ISC}$ and $M_{L,ISC}$ as given in equation (3.32) below

$$M_{L,ISC} = 1.219 * M_{N,ISC} - 0.972 \quad (3.32)$$

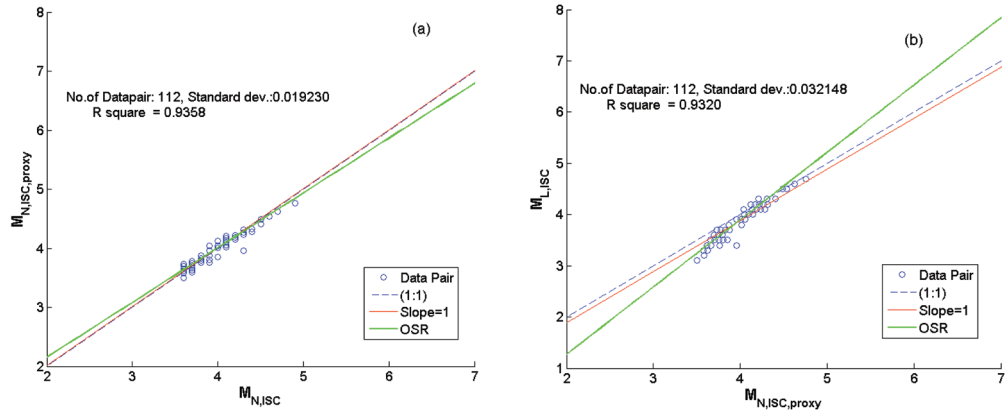


Figure 3.21

(a) OSR relation between $M_{N,ISC}$ and $M_{N,ISC,proxy}$ and (b) OSR relation between $M_{N,ISC,proxy}$ and $M_{L,ISC}$.

3.3.8 Relation between $m_{pv,ISC}$ and $m_{b,ISC}$

To develop a regression relation between $m_{pv,ISC}$ and $m_{b,ISC}$ for the magnitude range $3.4 \leq m_{pv,ISC} \leq 6.6$, we divided the dataset into two subsets. The first dataset comprising of 2029 randomly selected events have been employed to derive OSR relation and the second set consisting of 500 events have been used to validate the relation derived. Thus the OSR relations depicted in Figure 3.22 are worked out as

$$m_{pv,ISC,proxy} = 1.137 (\pm 0.0015) * m_{pv,ISC} - 0.547 (\pm 0.0061) \quad (3.33)$$

With $R^2 = 0.7942$, $\sigma = 0.038$ and $\eta = 1.0$.

$$m_{b,ISC} = 1.176 (\pm 0.0038) * m_{pv,ISC,proxy} - 0.9814 (\pm 0.015) \quad (3.34)$$

With $R^2 = 0.8255$ and $\sigma = 0.0424$.

From equations (3.33) and (3.34) we finally derived the OSR relationship between $m_{pv,ISC}$ and $m_{b,ISC}$ as given in equation (3.35) below

$$m_{b,ISC} = 1.337 * m_{pv,ISC} - 1.625 \quad (3.35)$$

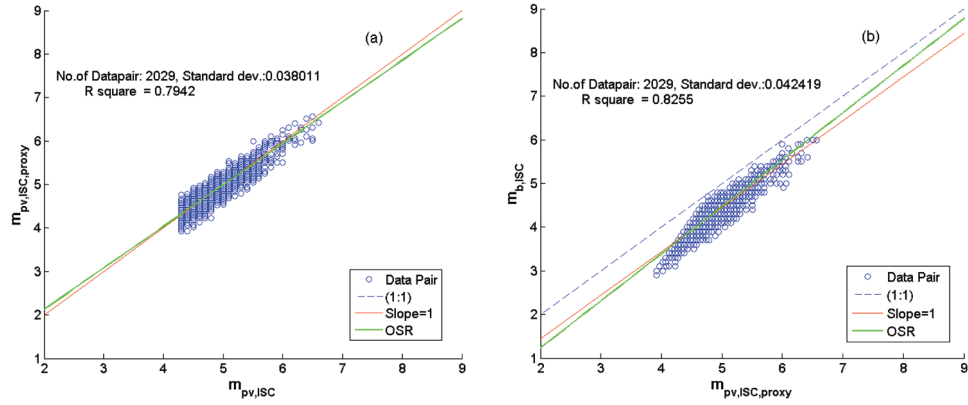


Figure 3.22

(a) OSR relation between $m_{pv,ISC}$ and $m_{pv,ISC,proxy}$, and (b) OSR relation between $m_{b,ISC}$ and $m_{pv,ISC,proxy}$

3.3.9 Relation between $M_{Lv,ISC}$ and $m_{b,ISC}$

To derive regression relation between $M_{Lv,ISC}$ and $m_{b,ISC}$ the entire magnitude range is divided into two subsets as the frequency plot depicts a bilinear trend. First one consists of 764 events for the magnitude range $2.0 \leq M_{Lv,ISC} \leq 4.5$ and the other comprises of 615 events for the magnitude range $4.6 \leq M_{Lv,ISC} \leq 7.6$.

For the magnitude range $2.0 \leq M_{Lv,ISC} \leq 4.5$, the derived OSR relation is as follows and is depicted in Figure 3.23(a)

$$M_{Lv,ISC,proxy} = 0.859 (\pm 0.0427) * M_{Lv,ISC} + 0.647 (\pm 0.1734) \quad (3.36)$$

With $R^2 = 0.7576$, $\sigma = 0.0517$ and $\eta = 1.0$.

The OSR relation between $m_{b,ISC}$ and the corresponding $M_{Lv,ISC,proxy}$ for 608 events depicted in Figure 3.23(b) is worked out as

$$m_{b,ISC} = 1.12 (\pm 0.018) * M_{Lv,ISC,proxy} - 0.734 (\pm 0.076) \quad (3.37)$$

With $R^2 = 0.7570$ and $\sigma = 0.0469$.

From equations (3.36) and (3.37) we finally derived the OSR relation between $M_{Lv,ISC}$ and $m_{b,ISC}$ as

$$m_{b,ISC} = 0.962 * M_{Lv,ISC} - 0.0009 \quad (3.38)$$

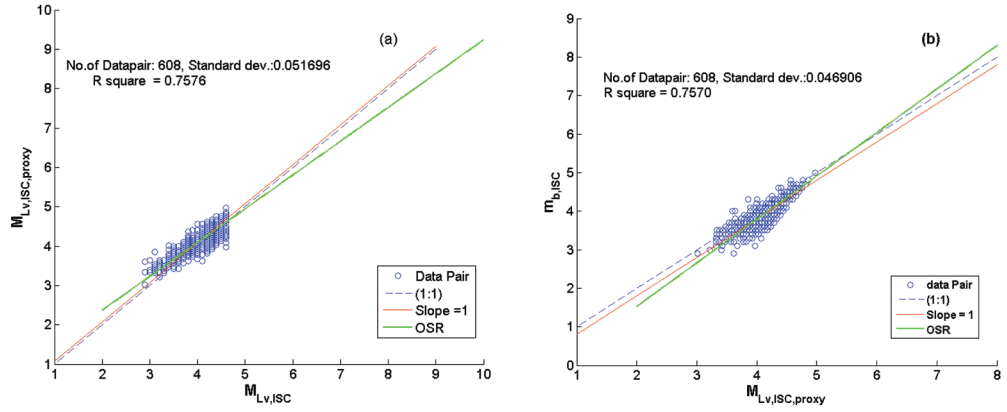


Figure 3.23

(a) OSR relation between $M_{L_v,ISC}$ and $M_{L_v,ISC,proxy}$, and (b) OSR relation between $M_{L_v,ISC,proxy}$ and $m_{b,ISC}$.

Similarly, the OSR relations for the magnitude range $4.6 \leq M_{L_v,ISC} \leq 7.6$ depicted in Figure 3.24 is given by

$$M_{L_v,ISC,proxy} = 0.853 (\pm 0.034) * M_{L_v,ISC} + 0.802 (\pm 0.179) \quad (3.39)$$

With $R^2 = 0.8480$, $\sigma = 0.036$ and $\eta = 1.0$.

$$m_{b,ISC} = 1.38 (\pm 0.041) * M_{L_v,ISC,proxy} - 2.5 (\pm 0.214) \quad (3.40)$$

With $R^2 = 0.8252$ and $\sigma = 0.052$.

Solving equations (3.39) and (3.40) we derived the OSR relation between $M_{L_v,ISC}$ and $m_{b,ISC}$ as

$$m_{b,ISC} = 1.177 * M_{L_v,ISC} - 1.393 \quad (3.41)$$

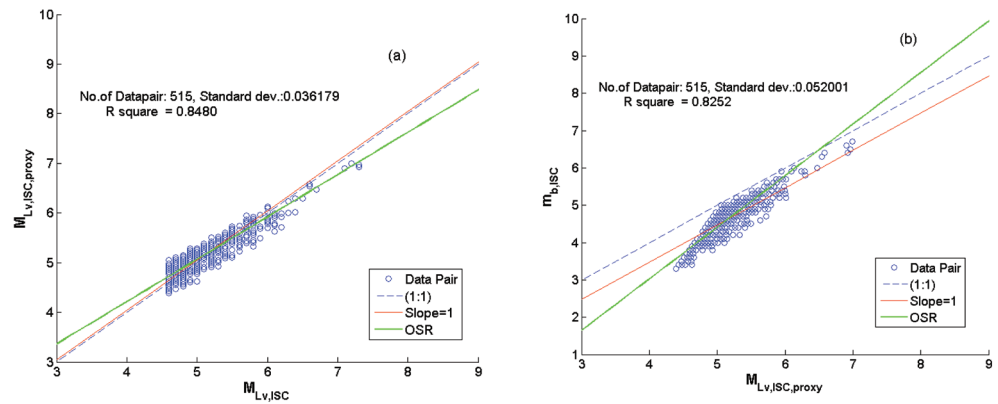


Figure 3.24

(a) OSR relation between $M_{L_v,ISC}$ and $M_{L_v,ISC,proxy}$, and (b) OSR relation between $M_{L_v,ISC,proxy}$ and $m_{b,ISC}$.

3.3.10 Relation between M_{ISC} and $M_{w,GCMT}$

The regression relation between M_{ISC} and $M_{w,GCMT}$ for the magnitude range $4.7 \leq M_{ISC} \leq 7.2$ using OSR method is depicted in Figure 3.25 and worked out as follows

$$M_{ISC,proxy} = 0.9719 (\pm 0.0286) * M_{ISC} + 0.1482 (\pm 0.1518) \quad (3.42)$$

With $R^2 = 0.9462$, $\sigma = 0.0206$ and $\eta = 1.0$.

$$M_{w,GCMT} = 1.0061 (\pm 0.0179) * M_{ISC,proxy} + 0.0143 (\pm 0.0950) \quad (3.43)$$

With $R^2 = 0.9410$ and $\sigma = 0.0212$.

From equations (3.42) and (3.43) we derived the OSR relation between M_{ISC} and $M_{w,GCMT}$ as

$$M_{w,GCMT} = 0.9778 * M_{ISC} + 0.1634 \quad (3.44)$$

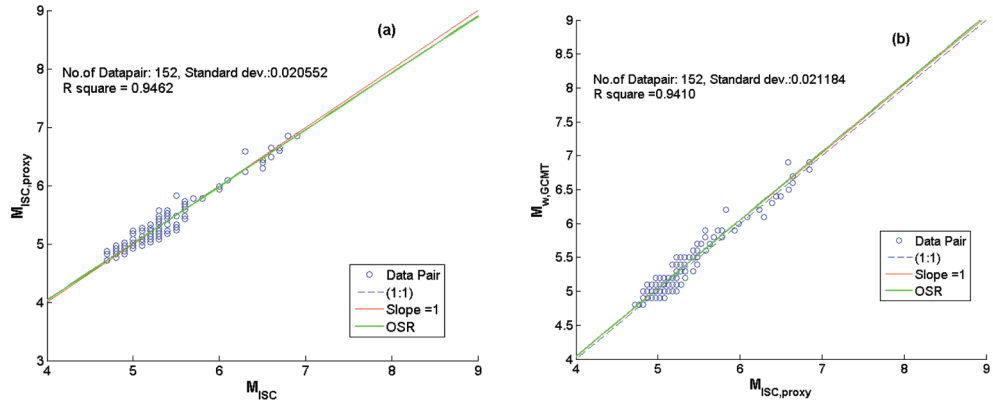


Figure 3.25

(a) OSR relation between M_{ISC} and $M_{ISC,proxy}$, and (b) OSR relation between $M_{ISC,proxy}$ and $M_{w,GCMT}$.

3.3.11 Relation between uk_{USGS} and $M_{s,ISC}$

To derive a relationship between uk_{USGS} and $M_{s,ISC}$, we considered 31 events in the magnitude range $6.5 \leq uk_{USGS} \leq 6.8$. A linear relationship (3.45) between uk_{USGS} and $M_{s,ISC}$ has been derived by least square fitting as depicted in Figure 3.26.

$$M_{s,ISC} = uk_{USGS} + 0.2 \quad (3.45)$$

$$R^2 = 1.0$$

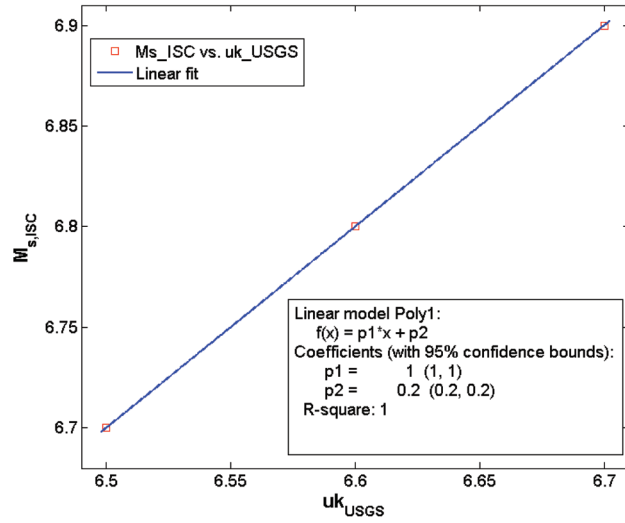


Figure 3.26

Linear relation between uk_{USGS} and $M_{s,ISC}$.

3.4 Data Compilation

3.4.1 Cataloging Process

To implement uniform magnitude scaling for the instrumental catalogue, the M_w entries found in GCMT are retained. The magnitude entry from ISC catalogue is selected maintaining a preference order of: $M_{s,ISC}$, $m_{b,ISC}$, $M_{L,ISC}$, $M_{D,ISC}$, $m_{pv,ISC}$, and $M_{Lv,ISC}$. Equation (3.4), along with the existing reported equations are used to convert $M_{s,ISC}$ into $M_{w,GCMT}$ for the magnitude range $3.5 \leq M_{s,ISC} \leq 6.6$. Equation (3.8) along with the existing reported equations are used to convert $M_{s,ISC}$ into $M_{w,GCMT}$ for the magnitude range $6.7 \leq M_{s,ISC} \leq 8.5$. Equation (3.11) along with the reported existing equations are used to convert $M_{s,USGS}$ to $M_{w,GCMT}$ for the magnitude range $4.5 \leq M_{s,USGS} \leq 5.6$. Similarly, Equation (3.14) is used to convert $M_{s,USGS}$ to $M_{w,GCMT}$ for the magnitude range $5.7 \leq M_{s,USGS} \leq 7.0$. Next $m_{b,ISC}$ is converted to $M_{w,GCMT}$ by using Equations (3.17) along with the reported existing equations. Equation (3.20) is used to convert $m_{b,USGS}$ into $M_{w,GCMT}$. $M_{L,ISC}$ is converted to $M_{w,GCMT}$ by using equations (3.23) along with the reported existing equations. Equation (3.26) along with the reported existing equations are used to convert $m_{w,USGS}$ into $M_{w,GCMT}$ for the magnitude range $5.1 \leq M_{s,ISC} \leq 7.0$. Equation (3.29) is used to convert $M_{D,ISC}$ into $m_{b,ISC}$. Equation (3.32) is used to convert $M_{N,ISC}$ into $M_{L,ISC}$. The entries given in $m_{pv,ISC}$ are converted to $m_{b,ISC}$ using equation (3.35) for the magnitude range $3.4 \leq m_{pv,ISC} \leq 6.6$. For the

magnitude range $2.0 \leq M_{L_v,ISC} \leq 4.5$ equation (3.38) is used to convert $M_{L_v,ISC}$ to $m_{b,ISC}$ while equation (3.41) is used for the magnitude range $4.6 \leq M_{L_v,ISC} \leq 7.6$ for the same. Equation (3.44) is applied to convert M_{ISC} to $M_{w,GCMT}$ for the magnitude range $4.7 \leq M_{ISC} \leq 7.2$. uk_{USGS} is converted to $M_{s,ISC}$ using equations (3.45) for the magnitude range $6.5 \leq uk_{USGS} \leq 6.8$. Rigsby *et al.* (2014) provided the equation for the conversion of $m_{bLg,USGS}$ into M_w . The uncertainties of the unified moment magnitude due to the usage of the conversion equations are incorporated during the compilation. Following Thingbaijam *et al.* (2009), likely duplication of events are eliminated by searching the events occurring on the same date, hour and minute within the spatial bound of 90 km, and retaining the one with the largest magnitude.

In order to assimilate the data from IMD into the present compilation, each record is correlated according to the date, time and reported epicenter manually. Only 306 events do not have a clear match with the entries of the ISC. However, Figure 3.27(a) indicates that the catalogue prepared by Jaiswal and Sinha (2004) have different magnitude coverage during the overlapped period with respect to the present compilation for the same spatial bounds. Figure 3.27(b) shows that M_w in the present study is, on an average, 0.095 units smaller implicating an uncertainty of 0.46 units with $M_{w,JS}$. Accordingly, we adopted a correction factor of - 0.095 and uncertainty of ± 0.46 units for the data source. Furthermore, we consult several reporting's to improve the data content. These include Pacheco and Sykes (1992), Chung and Gao (1995), Singh and Gupta (1980), Johnston (1993), Ambraseys and Bilham (2003b), Ambraseys and Douglas (2004), Mandal *et al.* (2004), Bilham *et al.* (2005), Wallace *et al.* (2005), Ulomov *et al.* (2006), Thingbaijam *et al.* (2008), and Amateur Seismic Centre (<http://asc-india.org/>).

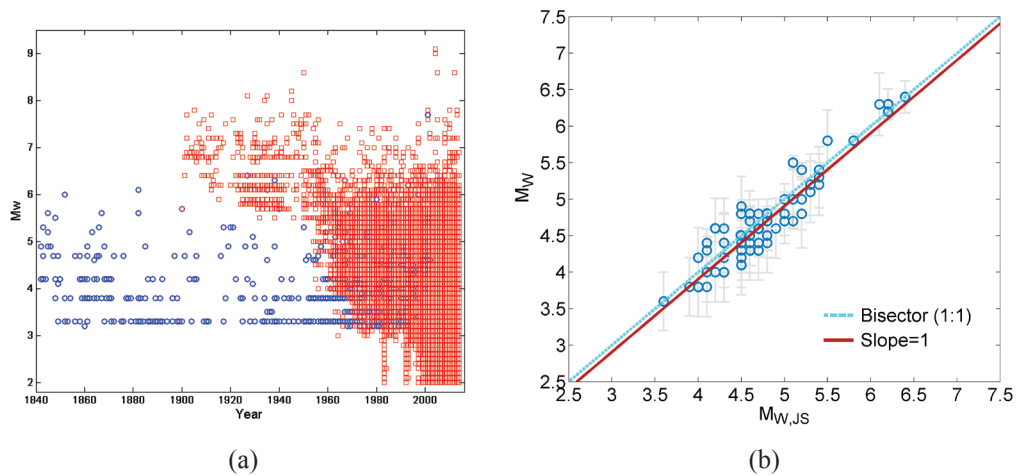


Figure 3.27

(a) The catalogue prepared by Jaiswal and Sinha (2004) vis-à-vis the present compilation, and (b) M_w show an overestimation of 0.095 units.

We adopt the following step-wise criteria for the entries:

1. The records derived using dataset from ISC are employed as primary data.
2. Any entry found to have a match in the dataset from USGS, it is replaced by the one obtained from USGS.
3. Entries in the dataset from USGS not found in the compilation (after step 2) are directly adopted in the compilation.
4. The combined ISC and USGS dataset thus generated, matched with the GCMT and events matched with GCMT entry is replaced by the one obtained from GCMT.
5. Entries in the dataset from GCMT not found in the compilation (after step 4) are directly adopted in the compilation.
6. If entry in Jaiswal and Sinha (2004) does not have a match in the compilation (after step 4), it is accepted into the compilation.
7. The events reported by IMD without any clear match with entries of the compilation (after step 6) are entered in the compilation.
8. Entries in the present compilation are updated with respect to the published reporting of magnitude in M_w , if available and are found to have one-to-one correspondence.
9. In case the reported event is not found in the compilation (after step 7), it is inserted into the compilation with appropriate magnitude scaling.

Eventually, we obtained a compilation with higher data volume compared to the original sources. Figure 3.28 depicts the corresponding spatial distribution of events.

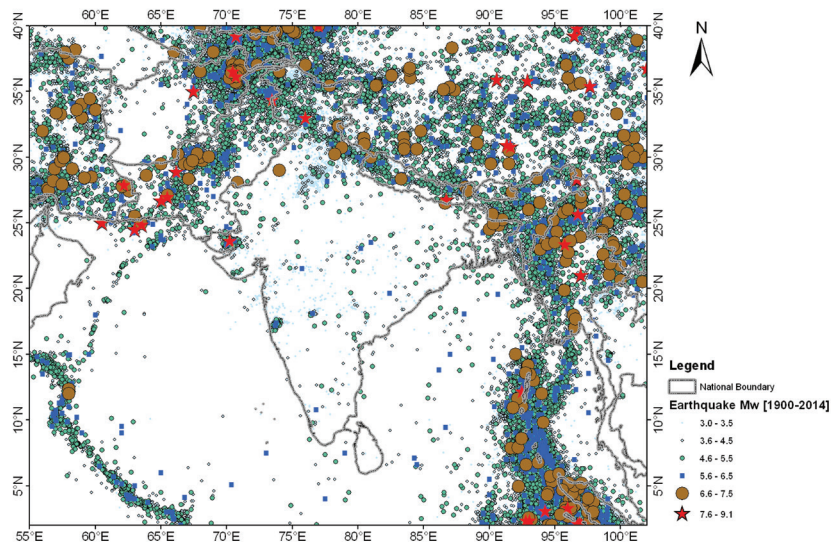


Figure 3.28

The seismicity map prepared using the compiled catalogue.

3.4.2 Seismicity Declustering

The space-time clustering of seismicity is mostly exhibited by foreshocks and aftershocks. Mainshock catalogues are derived by eliminating these clusters. Windowing algorithms are generally used for the purpose. The available algorithms (*e.g.* Gardner and Knopoff, 1974; Reasenber, 1985; Uhrhammer, 1986; Zhuang *et al.*, 2002; Hainzl *et al.*, 2006) generally differ in terms of the spatio-temporal window parameters. On the other hand, deciding optimal parameters is difficult in the light of diverse seismotectonic conditions (Gomberg *et al.*, 2003). In the present study we used the window based declustering algorithm of Gardner and Knopoff (1974) to identify aftershocks and foreshocks depending on inter-event space-time distance. According to Gardner and Knopoff (1974), the length and duration of the windows are given in the Table 3.8. This method does not consider secondary and higher order aftershocks.

We adopted this technique since (a) there is higher likelihood of aftershocks of larger mainshock events being recorded in the catalogue compared to those for the smaller ones, and (b) the spatial spans of aftershocks, especially for those associated with larger earthquakes, are dynamic depending not only on the magnitude of the event but also on the geological background.

Table 3.8

Aftershock identification windows (Gardner and Knopoff, 1974)

Magnitude	2.5	3.0	3.5	4.0	4.5	5.0	5.5	6.0	6.5	7.0	7.5	8.0
Distance (km)	19.5	22.5	26	30	35	40	47	54	61	70	81	94.0
Time (days)	6	11.5	22	42	83	155	290	510	790	915	960	985

The parameters listed in Table 3.8 are adopted for magnitudes $3.0 \leq M_{w,GCMT} \leq 8.0$, the aftershock zone is identified by inspecting continuous spatial windows of $0.25^\circ \times 0.25^\circ$ for the presence of at least one event within specified days limit corresponding to the main shock of a given magnitude. Once the zones are demarcated, the events found within the zone from the advent till the end of the catalogue are examined with cumulative number of events against time. Nyffenegger and Frohlich (2000) observed that the aftershock sequences for intermediate as well as deep earthquakes do not behave differently from those of the shallower ones. The algorithm, therefore, remains the same for the deeper (hypocentral depth ≥ 70 km) earthquakes and the termination of the aftershock sequences are decided accordingly. The analysis has uncertainties due to errors associated with epicentral locations, time and magnitudes. In the processing, the epicenters are grouped within a distance bound and consequently the errors associated are significantly reduced and so is with the case of time bins while the magnitude-wise correlation between the events is done with the assigned magnitudes. We restricted to the identification of the most likely aftershocks, and henceforth errors in the magnitudes are not given additional treatment. The same approach is used for the detection of likely foreshocks based on the increasing seismic activity. Finally, Figure 3.29 represents a seismicity map prepared using the derived mainshock catalogue.

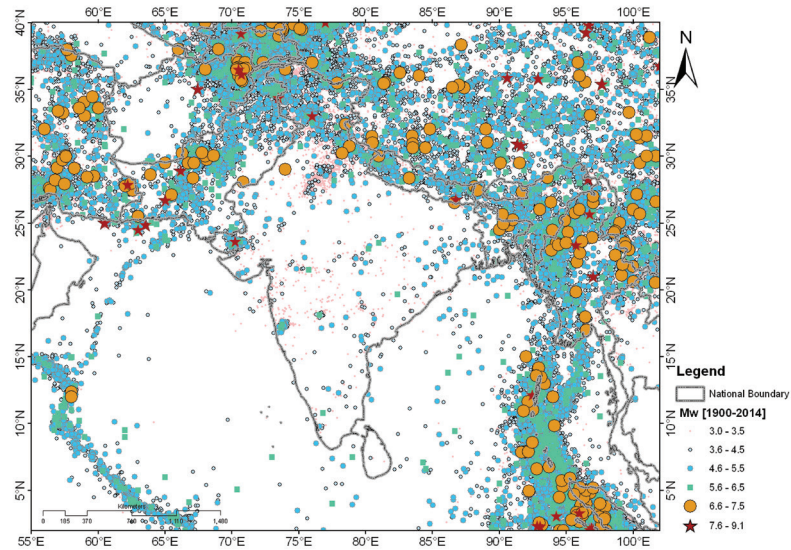
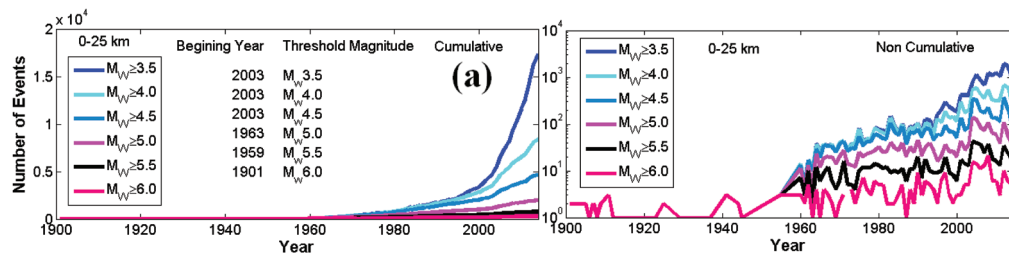


Figure 3.29

Declustered (Mainshock) seismicity covering a period 1900-2014 and comprising 58256 events.

3.4.3 Data Completeness

Earthquake catalogues are generally characterized by spatio-temporal heterogeneity in the data completeness mostly due to non-availability of relevant accounts or records as well as irregularities in the spatial and temporal coverage of monitoring networks. Quantitative assessment of data completeness is essential in order to facilitate unbiased estimate of background seismicity rates with the data segregated based on its completeness (*e.g.* Thingbaijam and Nath, 2008). Commonly applied statistical method considers time-independent seismogenic process to be stable (*e.g.* Stepp, 1972; Mulargia and Tinti, 1985). This decides the expected seismicity patterns or rather stability in the recordings but possibility not the completeness of the entire dataset (Albarello *et al.*, 2001). The fundamental hypothesis is that the mainshock events follow Poissonian behavior, and thereby, the data completeness test is essentially applicable for the declustered catalogues.



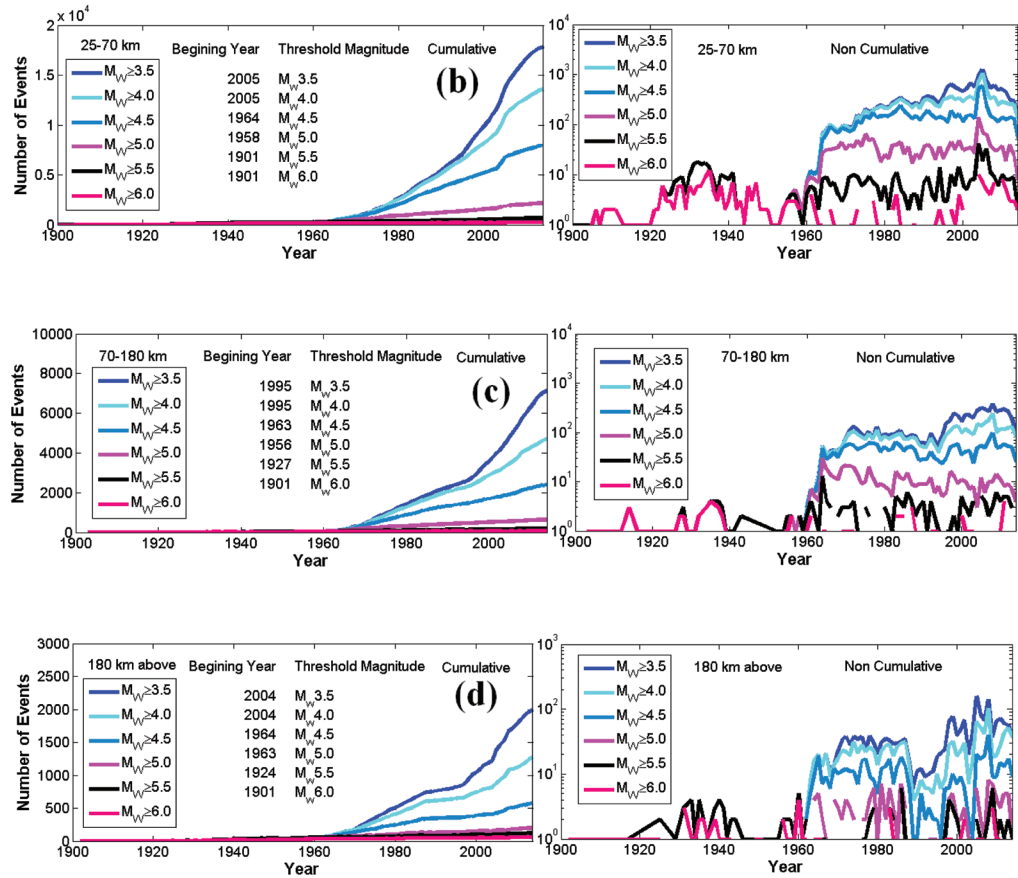


Figure 3.30

Data completeness plot (cumulative and non-cumulative) for the hypocentral depth (a) 0-25 km, (b) 25-70 km, (c) 70-180 km, and (d) 180 km below.

Presently we look at the broad regional level to achieve a groundwork assessment of the temporal variation of data completeness of the catalogue using the method employed by Mulargia and Tinti (1985). Minimum magnitudes at which stable seismicity is observed (referred to here as ‘threshold magnitude’) are inferred from constant average slope from the plot of cumulative number of events against time, which runs to the end of the catalogue. We also make use of non-cumulative plots for corroborative evaluations. Figure 3.30(a-d) depicts the data completeness plots for different hypocentral depths *i.e.* 0-25 km, 25-70 km, 70-180 km and below 180 km for the period 1900-2014. The data completeness is observed to have improved in all the cases during the last three decades.

3.5 Concluding Remarks

The spatial context of the relationships is constrained by the spatial coverage of datasets. The source spectral properties across different tectonic provinces, *e.g.* active subduction zones of Hindukush–Pamir, stable mid-plate regions, and normal-faulting type dominated ridge zone, entail different waveform properties that are source dependent. However, we could not establish any statistically significant diversity in the relationships between the different magnitude types. This may be due to the lack of definite tectonic class for a given region but the uncertainties have been specified by the standard deviation defined on the model parameters. The relations of $M_{s,ISC}$, $m_{b,ISC}$, $M_{L,ISC}$ and $m_{w,USGS}$ with $M_{w,GCMT}$ are seen to be consistent with the previous ones.

According to Sitharam and Borah (2007), $M_{L,ISC}$ and $M_{D,ISC}$ correspond to each other within an uncertainty margin of 0.25 units based on a local database from Northeast India. A linear relation between $m_{bLg,USGS}$ and M_w has been derived by Rigsby *et al.* (2014) for Eastern North America. On the other hand, higher difference of 0.46 units has been observed between $M_{w,GCMT}$ and $m_{b,ISC}$ by Braunmiller and Nábelek (2002) for the explorer region. The correlations between $m_{b,ISC}$ and $m_{pv,ISC}$ agree well with those given by Thingbaijam *et al.* (2009). The connections of different magnitudes are summarized in Figure 3.31. It is seen that all the magnitude types (excluding $M_{s,USGS}$ and $m_{L,ISC}$) converges at M 5.5.

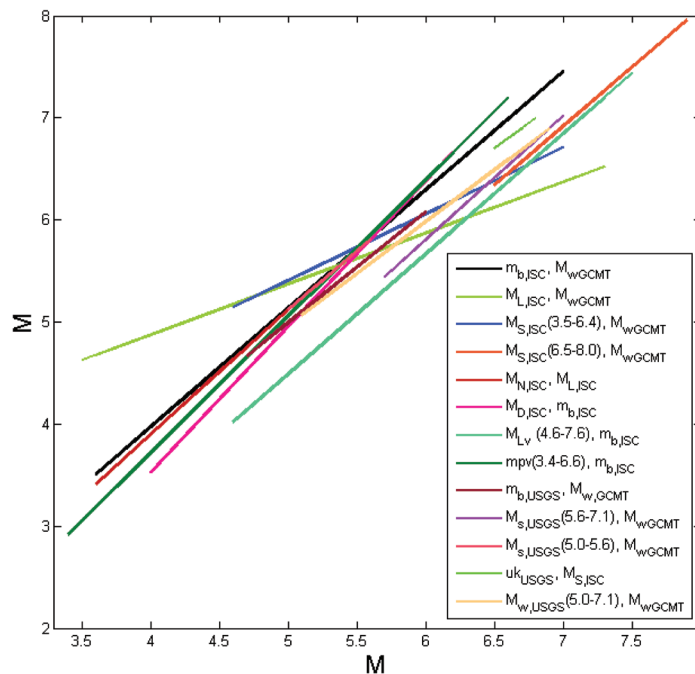


Figure 3.31

The relations for different magnitude types derived in the present study.

We performed a first order declustering of catalogue by eliminating likely aftershocks and foreshocks, to enable a groundwork assessment of the temporal variation of data completeness. Further analysis on the aftershocks and foreshocks would involve complex models such as Epidemic Type Aftershock Sequence (ETAS, Ogata and Zhuang, 2006) with recursive inspections on each aftershock event for secondary aftershocks. We observed a drastic increase in the number of events after 1964 accompanied by an increased number of foreshocks and aftershocks in the data volume. This can be attributed to improved instrumentation. The application of constant slope check on the plots of cumulative number of events against time indicates that overall data completeness has considerably improved since the last two decades.

Thus the complete and homogeneous earthquake catalogue prepared for Southeast Asia provide the basic requirement for earthquake induced disaster management and mitigation purpose in terms of seismicity analysis, seismic hazard, vulnerability and risk assessment.

